



Contents lists available at ScienceDirect

Journal of Constructional Steel Research

journal homepage: www.elsevier.com/locate/jcsr

Evaluation of a steel railway bridge for dynamic and seismic loads

Ozden Caglayan, Kadir Ozakgul*, Ovunc Tezer, Erdogan Uzgider

Department of Civil Engineering, Istanbul Technical University, 34469 Maslak, Istanbul, Turkey

ARTICLE INFO

Article history:

Received 3 March 2010

Accepted 20 February 2011

Keywords:

Railway bridge
Bridge assessment
Field testing
Model calibration
Safety index
Impact factor

ABSTRACT

In this study, dynamic and seismic assessment of a railway bridge system with four discrete spans giving service on a double track railway line and located in an earthquake-prone region in Turkey is presented. A three-dimensional computer model of the bridge was generated using a commercial general finite element analysis software. Field measurements such as static and dynamic tests as well as material tests were conducted on the bridge system. Validation of the finite element model was performed based on the results of these tests. The calibrated 3D model of the bridge structure was then used for necessary calculations regarding structural assessment and evaluation according to train loads as well as seismic loads. Additional members were proposed to transmit seismic loads to supports. The fourth span, which had a permanent imperfection due to truck collision was studied in detail. Results have shown that due to excessive amount of capacity loss, the only choice was to write off the fourth span.

© 2011 Elsevier Ltd. All rights reserved.

1. Introduction

Most existing railway bridges giving service on current railway networks may not be capable of carrying the heavy vehicles of modern traffic, although no apparent signs of structural deficiencies are observed. However, studies demonstrate that there are large differences between the actual load carrying capacities of bridges and those predicted by conventional theory. To get the maximum use out of a bridge, its assessed load carrying capacity should be safely close to its actual resistance. For evaluating the safety of a bridge, safety index and rating factors are used. Actual reduced capacity of deteriorated members and the maximum loading due to the most critical composition and volume of heavy traffic that may be projected for the future affect these two safety parameters.

Assessment of a railway steel truss bridge by using a validated computer model that was developed based on dynamic field measurements and laboratory tests was conducted by Ermopoulos and Spyrakos [1] under heavier train loads as well as seismic and wind loads with regard to current design codes. In another experimental and analytical study of a historic railway bridge by Spyrakos et al. [2], seismic and wind load carrying capacities of the bridge were evaluated based on the analytical model validated with static and dynamic field measurements and laboratory tests. Schlune et al. [3] proposed a methodology for finite element model updating for improved bridge evaluation and this methodology was applied to one of the world's largest single-arch bridges. For numerous existing small and medium single span ballasted railway bridges in Austria, dynamic field measurements were performed by Rebelo et al. [4] and the calibration of the finite element

models of these bridges was carried out using the measured modal parameters. Calçada et al. [5] conducted the experimental and numerical dynamic analyses of Luiz I Bridge, an old arch and double-deck iron bridge in Lisbon, to obtain an experimentally calibrated finite element model of the bridge structure. Full-scale ultimate load tests were carried out by Maragakis et al. [6] on a typical ballasted railway bridge, located in Los Angeles, to identify the contribution of bridge components during a seismic event. Chajes et al. [7] presented results of experimental load tests on a three-span, steel girder-and-slab bridge and generated a finite element model of the main span using the measured response of the bridge and using this calibrated model, various load ratings for the bridge were determined. Wang et al. [8] summarised a condition assessment procedure for bridges based on a complete system of field-testing, finite element modelling and load rating. A study was conducted by Akgul and Frangopol [9] on the rating and system reliability-based lifetime evaluation of a number of existing bridges within a bridge network, including pre-stressed concrete, reinforced concrete, hot-rolled steel and steel plate girder bridges. Itani et al. [10] discussed the behaviour of steel plate girder bridges during recent earthquakes and the experimental and analytical investigations that were conducted on steel plate girder bridges and their components. Results of these investigations show the importance of shear connectors in distributing and transferring the lateral forces to the end and intermediate cross frames.

In this study, assessment of a railway steel bridge was conducted for train and seismic loads according to relevant specifications. A three-dimensional computer model of the bridge was generated and validated based on dynamic field measurements and laboratory tests. The calibrated 3D model of the bridge structure was then used for necessary calculations regarding structural assessment and evaluation.

* Corresponding author. Tel.: +90 212 2853813; fax: +90 212 2856587.
E-mail address: ozakgulk@itu.edu.tr (K. Ozakgul).



Fig. 1. A general view of the bridge.

2. Description of the bridge

The bridge is located approximately 10 km from historical Sirkeci railway station which is the starting point of Europe-directed railway track in Istanbul. It was designed and built in late 1960s by TCDD (Turkish Railways Administration) which is the governmental authority of the country. The bridge is situated in metropolitan area of the city and is subject to heavy traffic of passenger transportation, mainly suburban commuter trains. As shown in Fig. 1, the bridge is composed of four simply supported spans, each with riveted steel plate girders, an open deck, stringers and cross beams. The layout of the bridge is given in Fig. 2. Each span has a length of 13.5 m.

The railway bridge passing over the divided two-way street has been damaged due to truck collisions caused by overloaded trucks passing underneath. Most of the damage has occurred on the lateral cross bracing system of almost all four simple spans (see Fig. 3), the fourth span also has damage at the upper and lower flange of its main girder. However, there is almost no damage on the main girders at other spans. This damage in the fourth span main girder has resulted in a permanent imperfection of maximum 12 cm of lateral deformation at the midspan, as shown in Fig. 4.

3. Material tests for steel

Tension and Charpy-V-notch impact tests were conducted on specimens extracted from damaged horizontal braces.

Table 1
Results of tension test.

Specimen no.	Yield strength (MPa)	Tensile strength (MPa)
1	212.6	367.2
2	239.9	389.7
3	239.7	389.2
4	264.2	405.9
Mean value	238.1	388.0
Standard deviation	21.1	15.9
Nominal value	217.0	372.1

Table 2
Charpy-V-notch test results.

Specimen no.	Charpy-V-notch energy (J)
1	40
2	40
3	43
Standard deviation	1.73

3.1. Tension test

Four specimens were used during tension tests. After having prepared the specimen according to ASTM standards [11], tension tests were conducted to identify the material quality used in construction. Results are presented in Table 1. As is seen from the evaluation of the data from Table 1, bridge material can be classified as S235 quality structural steel.

3.2. Charpy-V-notch test

Charpy-V-notch tests have been conducted for the three specimens taken from the bridge members at room temperature. Test results are given in Table 2. It is clearly seen that obtained results are quite satisfactory.

4. Field tests

Free vibration and quasi-static tests were conducted on bridge spans to understand the actual behaviour of the bridge superstructure. Member sizes were also checked and verified according to constructional drawings.

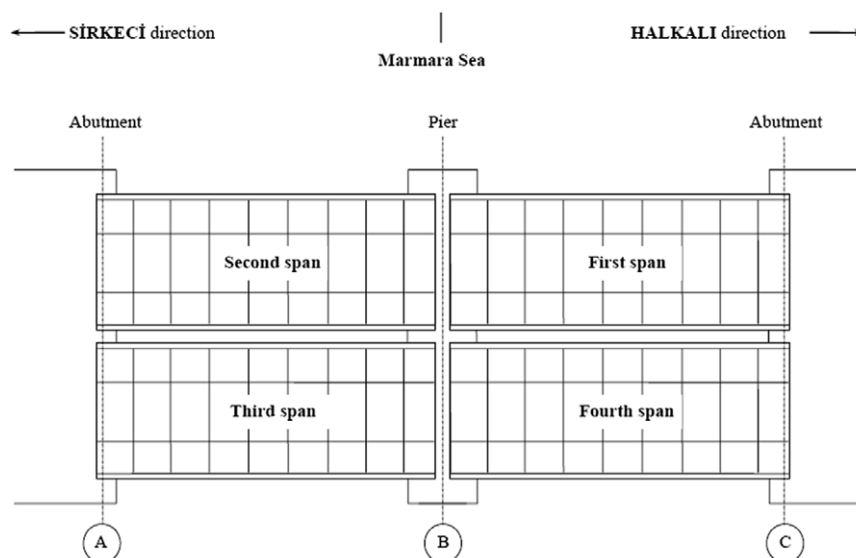


Fig. 2. Layout of the bridge.



Fig. 3. Buckled cross braces under the fourth span.



Fig. 4. Deformed main girder of the fourth span.

4.1. Quasi-static tests

These tests were performed for calibrating the computer model. Also matching the strain values of actual bridge components and corresponding elements of the computer model was aimed. During

tests, all four spans of the bridge were loaded by an E43000 type locomotive. For each span, reusable Hottinger Baldwin (HBM) made DS-5 type strain transducers were mounted on bridge members at specific locations, as shown in Figs. 5–7.

Two portable NEC computer-based dynamic data acquisition systems having 16 channels each with an 800 sps sampling rate for each channel were used to collect strain data while an E43000 type locomotive was loading the bridge with a crawling speed of approximately 5 km/h. A schematic description of the data acquisition system is given in Fig. 8.

To simulate moving load in the computer model, axle loads and axle spacings for the E43000 type locomotive according to fabricator's documents were used. After the tests, it was possible to display the collected strains as a function of load position. All the strain data recorded in the field were filtered to separate the dynamic component from the recorded data to obtain the static component and these strains were converted to stress values as shown in Fig. 9.

4.2. Free vibration tests

These tests have been conducted mainly for obtaining data to define the dynamic characteristics of the bridge system and for prediction of any existing damage.

During tests, SA-102 model accelerometers manufactured by Terra Technology Corporation were used. Two accelerometers were mounted on the stainless steel base angles having three short pointed legs for stable placement on a rough surface to obtain a biaxial accelerometer unit which is able to measure in vertical and horizontal directions. Installation of the accelerometers on the floor beam upper flanges is shown in Figs. 10 and 11 for each span.

Free vibration after the locomotive induced loading (see Fig. 12) was used for assessment of the dynamic characteristics of the bridge. Since acceleration recordings in their raw form (see Fig. 13) do not provide a good identification of the system, a much better identification of modal parameters can be realised if collected acceleration data are pre-processed prior to identification. Pre-processing involves removal of mean, existing trends, noise contaminations and outliers, filtering, decimation and synchronisation of the collected data.

5. Computer modelling of existing bridge

A three-dimensional computer model covering almost all significant structural irregularities and stiffness changes that exist on the bridge structure was prepared. A single span was modelled with beam and spring elements using the general-purpose finite element analysis software COSMOS/M [12], as given in Fig. 14.

Two riveted plate girders functioning as the main girder of each span were simulated with $i-i$ and $ii-ii$ beam elements located

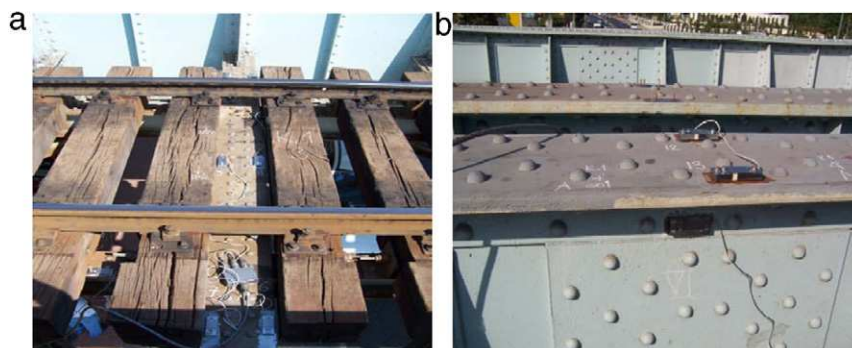


Fig. 5. Strain transducers mounted on (a) stringers and cross beams (b) a main girder.

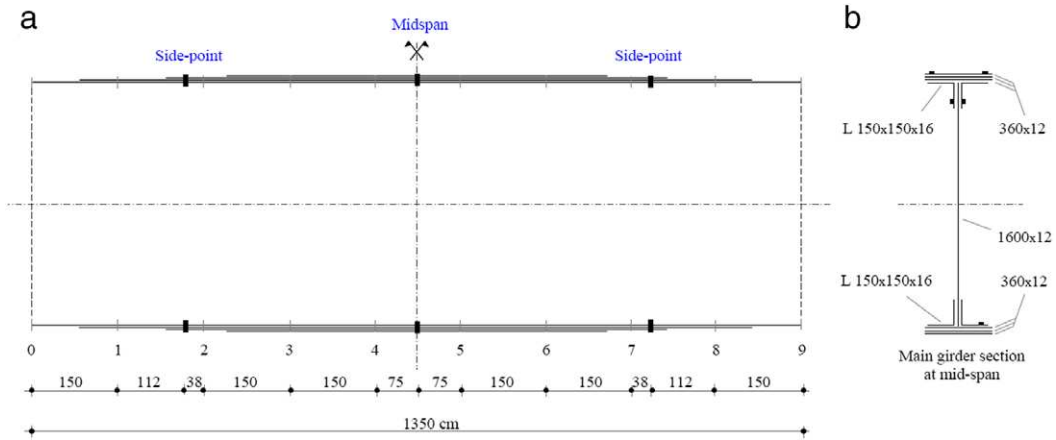


Fig. 6. Locations of the strain transducers on a main girder (a) on the longitudinal direction (b) on the cross section.

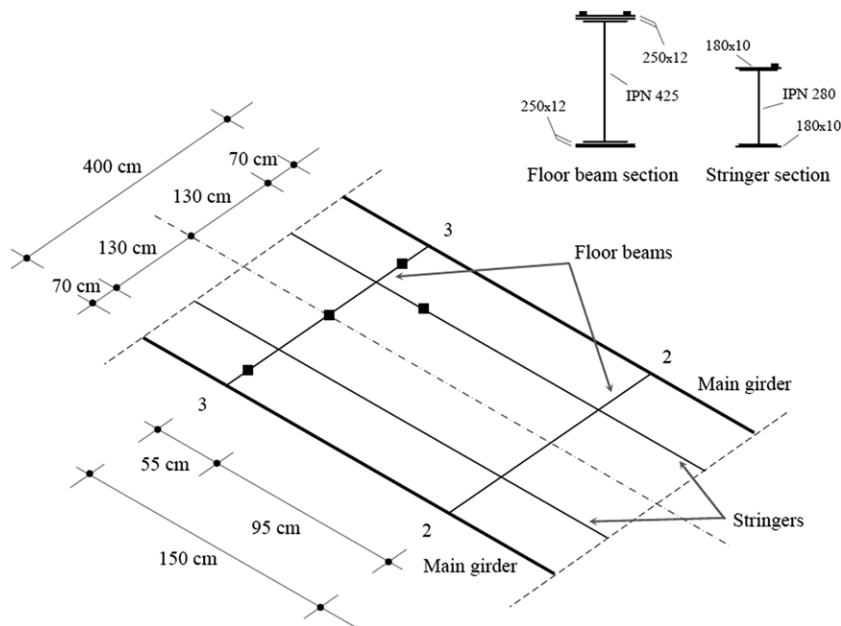


Fig. 7. Locations of the strain transducers on the floor beams and the stringers.

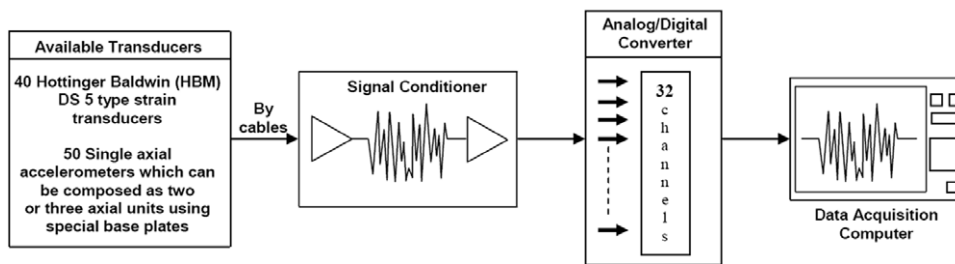


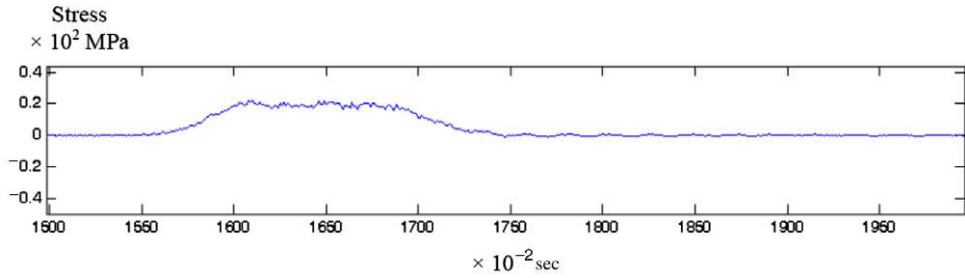
Fig. 8. Schematic description of the data acquisition system.

on the centroid line and having the same torsional and flexural rigidities of actual main girders (see Figs. 14 and 15).

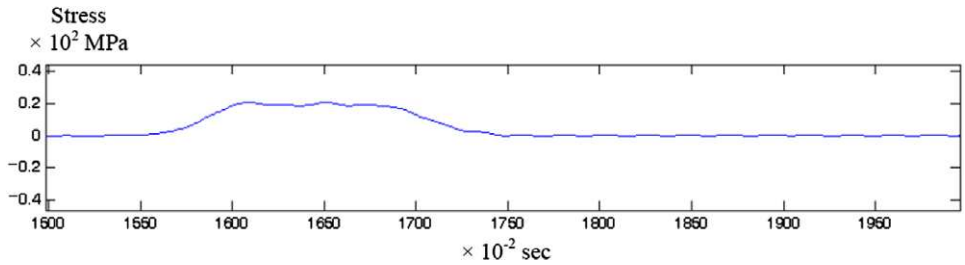
Floor beams were modelled by using beam elements between points *c-c* in the transverse direction and rigid bars were used between points *c* and *c'* that simulate centre of gravity for floor beams and main girders, respectively. Since the connections between the rigid bars and cross beams are semi-rigid rather than fixed, springs are used to simulate joint rotational rigidities. The *j-j* and *jj-jj* line elements having no flexural rigidity simulate the axial rigidities provided by main girder lower flanges. Connections

between the rigid bars and all of the line elements (*i-i*, *ii-ii*, *j-j* and *jj-jj*) are free to rotate in the longitudinal vertical plane as seen in Fig. 14. Also the connections between the stringers and cross beams behave semi-rigidly, therefore rotational spring elements are used to simulate the rotational rigidities (see Fig. 14).

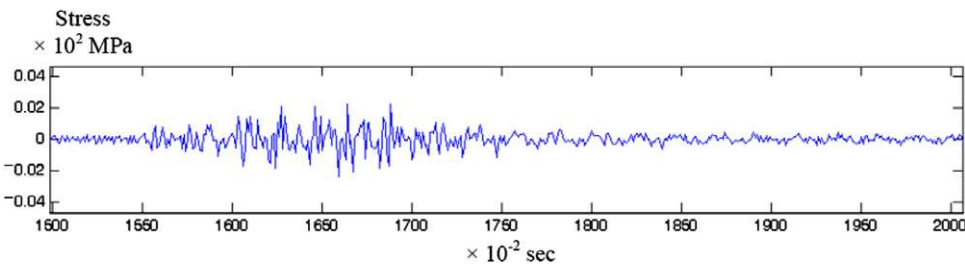
Moreover, vertical, transverse and longitudinal spring elements for each main girder support were included in the model to simulate the effective stiffness of the combined bearing and pier or abutment structure and the longitudinal restraints at the sliding bearings in each direction.



(a) Recorded stress trace.



(b) Static component.



(c) Dynamic component.

Fig. 9. Dynamic and static components of recorded stress traces.

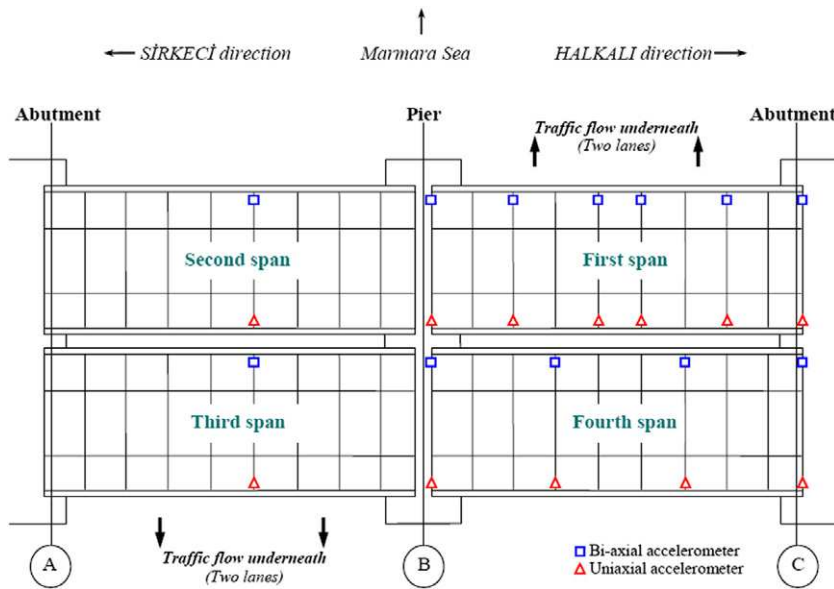


Fig. 10. Positions of accelerometers.

6. Validation of the computer model

Acquired strain data from quasi-static tests were processed to separate the dynamic component from the recorded data so as to obtain the static component. These strain data were used to

obtain a refined computer model that will yield strains having high correlation with the actual bridge structure.

In order to accomplish this, a systematic optimisation scheme was utilised to adjust the structural rigidities such as flexural, axial and torsional rigidities, spring constants in an automated

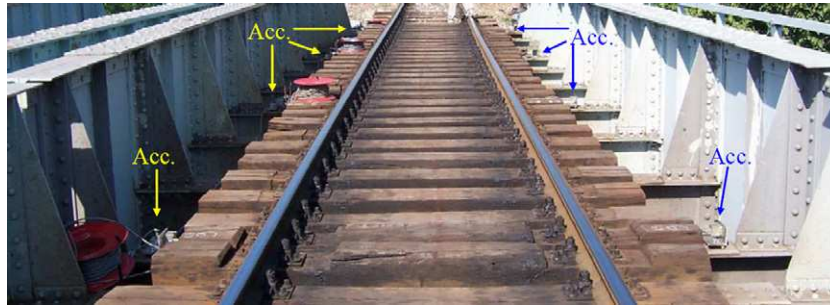


Fig. 11. Layout view of accelerometers on the fourth span.



Fig. 12. Dynamic loading by E43000 type electrical locomotive.

fashion to refine the initial computer model. In this procedure, an objective function was considered as the sum of squares of

the differences between the measured and analytically obtained stresses for appropriate strain transducer locations, as given in Eq. (1),

$$J = \sum_{k=1}^n (\sigma_k^a - \sigma_k^e)^2 \quad (1)$$

where n = number of strain transducer locations considered, σ_k^a = analytically obtained stress using initial computer model for n transducer locations, σ_k^e = experimentally obtained stress values for n transducers.

The above mentioned scalar objective function is minimised by changing the optimisation parameters (stiffness parameters presumed during preparation of the initial computer model). After the appropriate values for the optimisation parameters are selected by this process, the refined computer model of the bridge is obtained. In Figs. 16 and 17, measured stress traces and analytically obtained stress traces using initial computer model are shown with continuous blue and green dashed curves, respectively. On the same figures, the stress traces obtained analytically by employing a refined computer model are represented by red dashed curves.

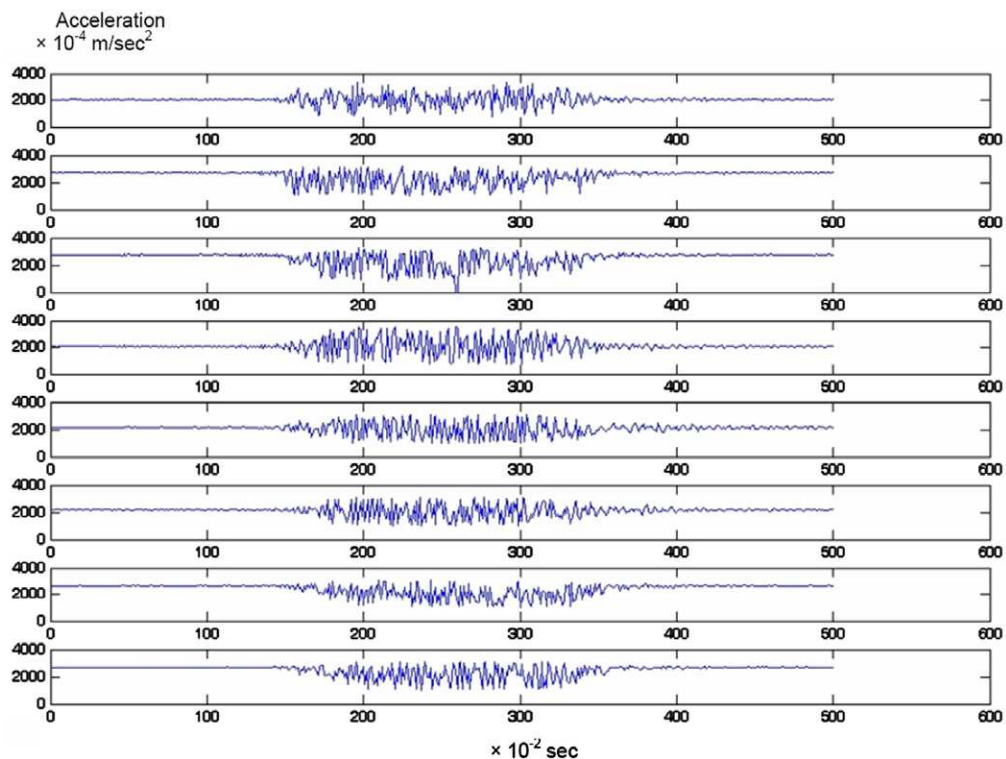


Fig. 13. Typical acceleration records.

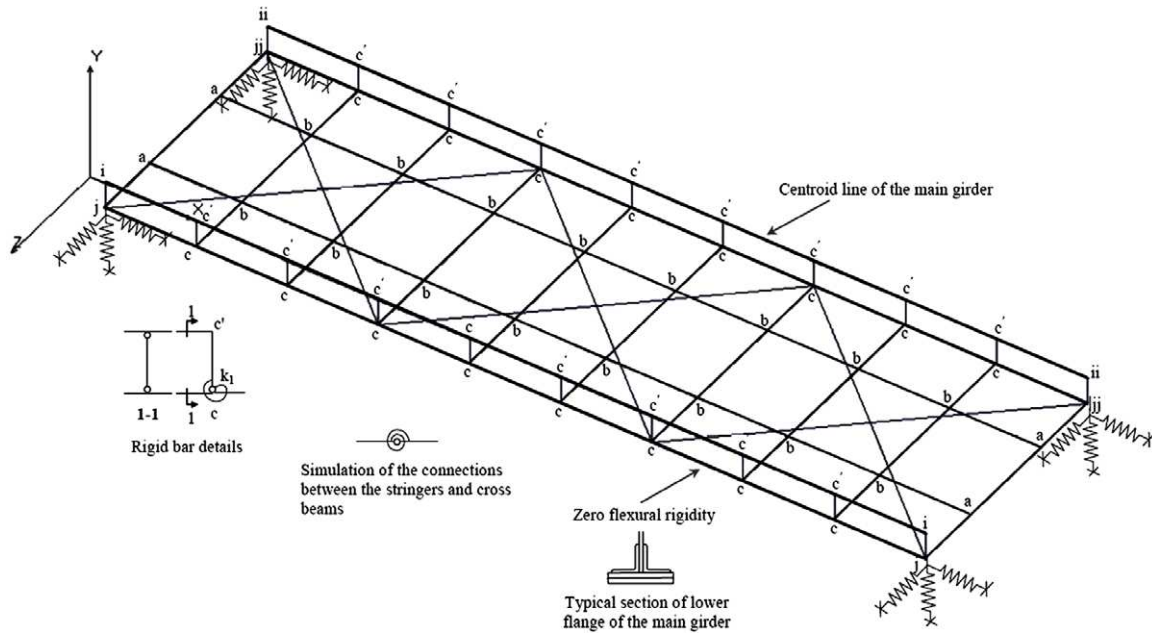


Fig. 14. 3D computer model of the bridge.

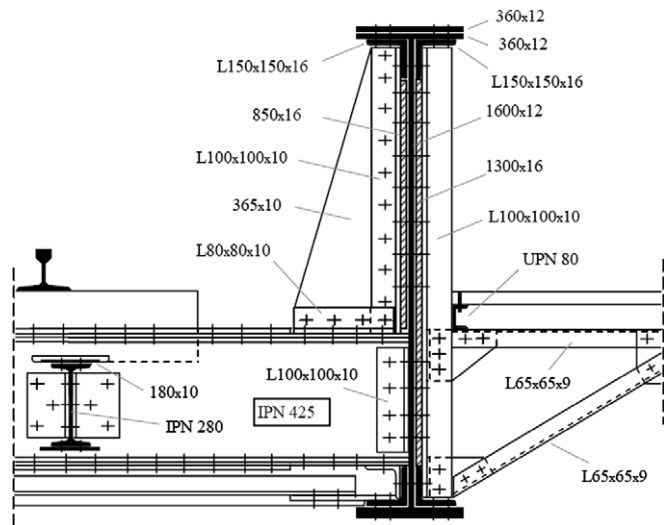


Fig. 15. Detail of floor beam to main girder connection.

Table 3

First modal frequencies for the spans.

Span no.	Analytically obtained (Hz)	Experimentally obtained (Hz)
1	19.05	18.99
2	19.05	18.95
3	19.05	19.09
4	19.05	16.60

First modal frequencies for each span obtained by using an updated finite element model and by the collected acceleration data are given in Table 3.

7. Rating of load carrying capacity

The rating procedure was performed for the load profile defined by UIC standards [13] considering the updated computer model of the bridge. Rating factors (RF) are computed for the most critical members against failure as,

$$RF = \frac{F_y}{\gamma\omega} - F_g \quad (2)$$

in which, F_y is yield stress of the bridge material, γ is the safety factor used for the allowable stress design [14], φ is the impact factor, ω is the dimensionless buckling coefficient [15], F_g is the stress for each element under dead load, F_p is the stress for each element calculated for the selected train load profile. An allowable stress design approach is used with regard to former versions of modern design codes as these former versions are still in use and are mandated by the local authorities. However, a thorough upgrade of these codes is under progress.

The impact factor, φ is taken as the ratio of the maximum dynamic strain and the maximum static strain obtained by filtering the dynamic strain [16], as follows,

$$\varphi = \frac{\epsilon_{dyn}}{\epsilon_{stat}} \quad (3)$$

where, ϵ_{dyn} is the absolute maximum dynamic strain under the vehicle travelling at normal speed, and ϵ_{stat} is the maximum static

6.1. Identification of modal parameters

In order to define modal parameters, after the collected acceleration data from each accelerometer were preprocessed, acceleration spectra were obtained by using the Fast Fourier Transform (FFT) technique, as shown in Fig. 18. Then, the first-mode frequency and corresponding mode shape were defined for the spans.

The mode shapes and frequencies obtained from the initial computer model were compared and in case of considerable difference, model updating was performed by altering rotational and translational rigidities of spring elements. Employing modal identification procedures, the first mode of vibration for each span was identified. The first mode of vibration obtained from the refined computer model is shown in Fig. 19. For comparison, mode shapes defined based on the collected acceleration data are shown by blue curves and the corresponding mode shapes obtained analytically using a refined computer model are shown by red curves for the first and fourth spans (see Fig. 20).

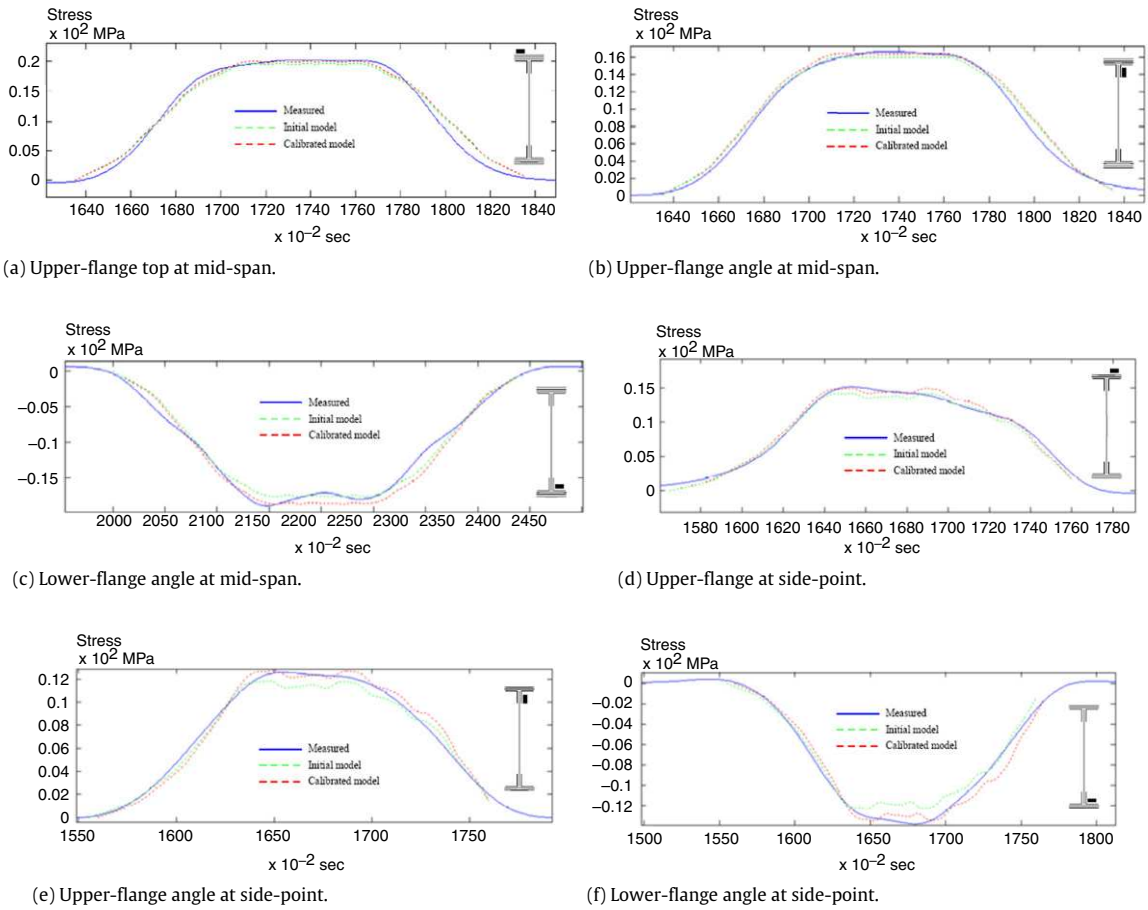


Fig. 16. Stress traces for main girder.

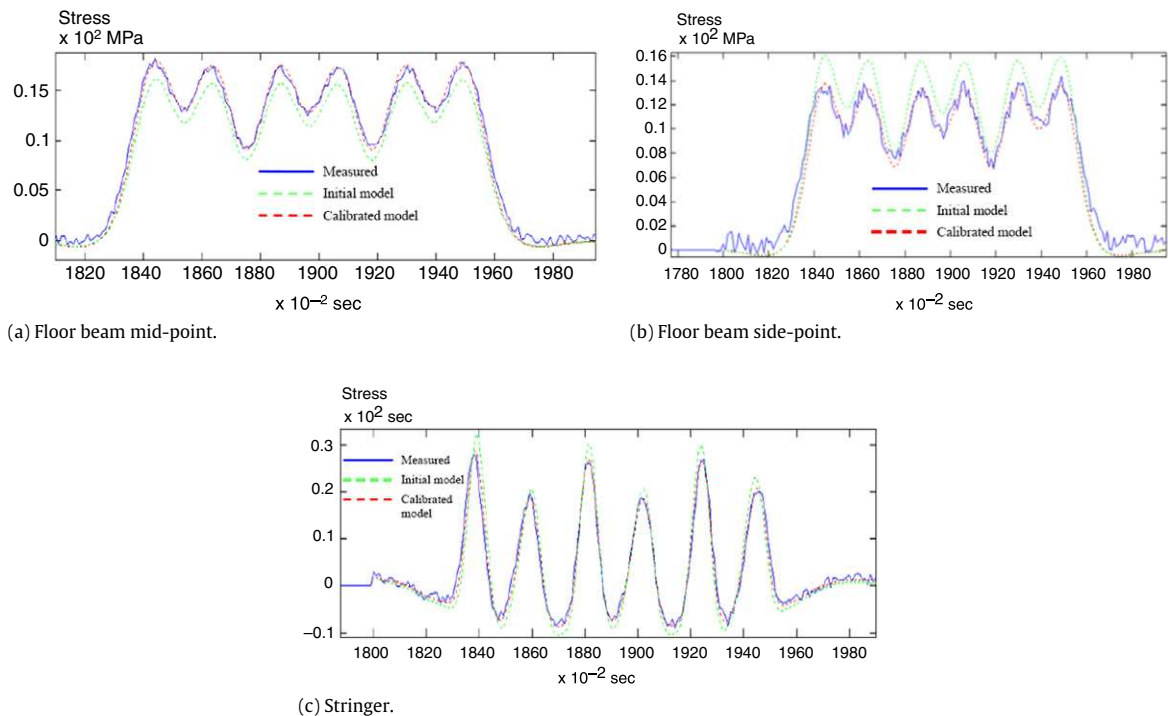


Fig. 17. Stress traces for floor beam and stringer.

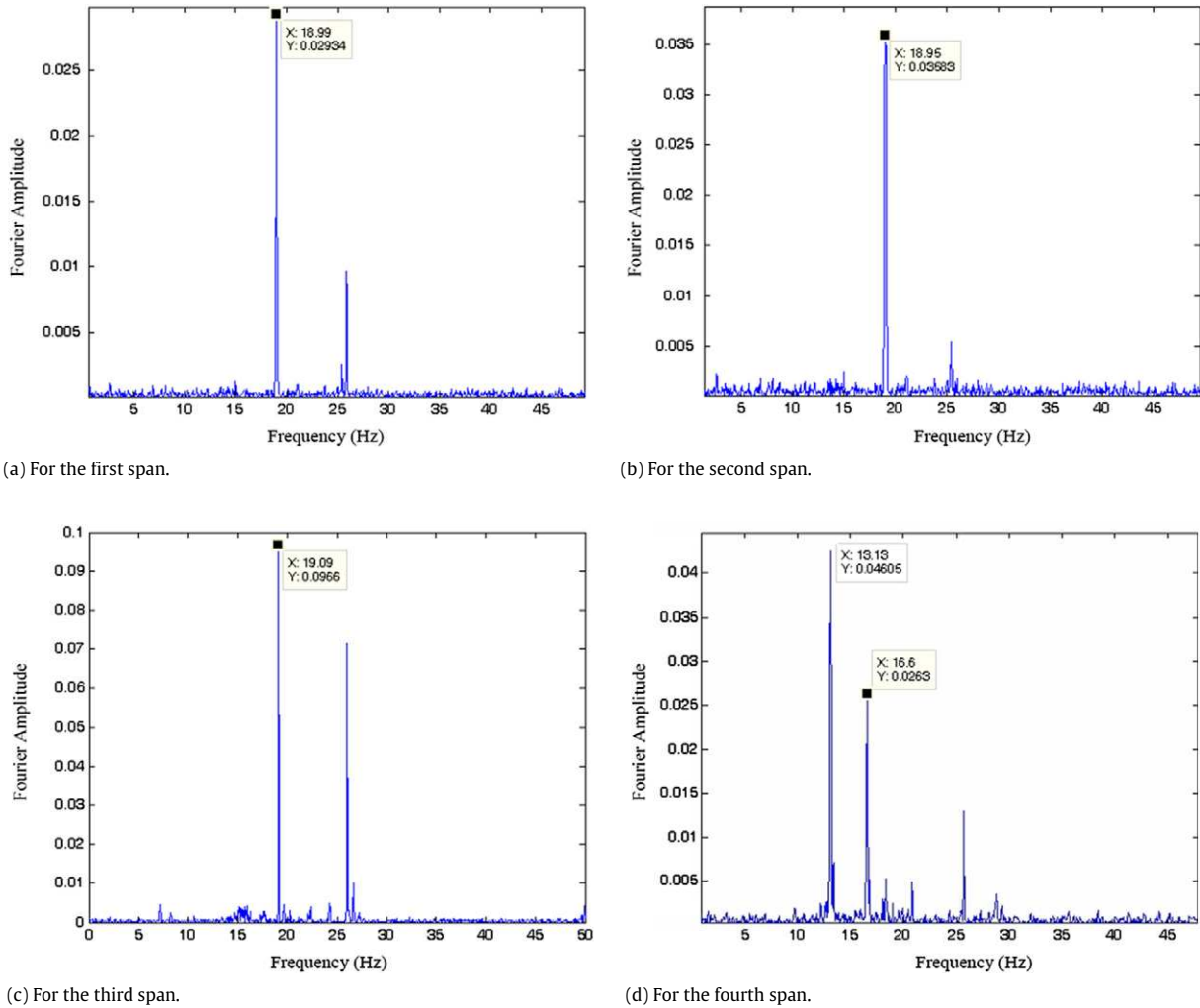


Fig. 18. Acceleration spectrum for each span.

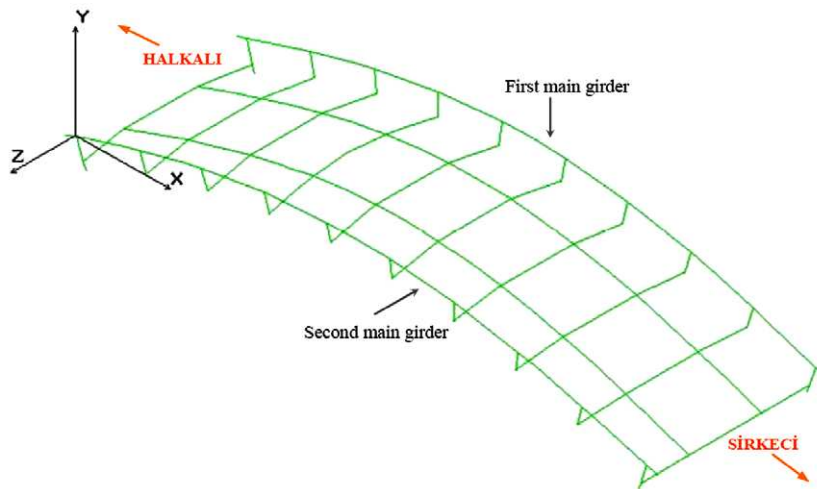


Fig. 19. Identified mode shape by computer model.

strain obtained by filtering the dynamic strain. The values for impact factors for various structural elements are presented in Table 4.

The normal distribution of a random variable is the most important statistical distribution in structural reliability theory. As seen in Fig. 21, probability density functions $f_R(r)$ and $f_Q(q)$

for normal random variables R and Q are given. R represents the resistance and Q represents the load effect. Sometimes R is thought of as capacity and Q is taken as demand. A performance function, or limit state function can be defined for failure as,

$$g(R, Q) = R - Q. \tag{4}$$

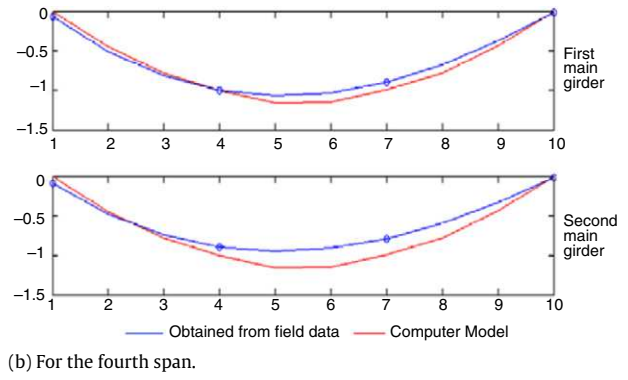
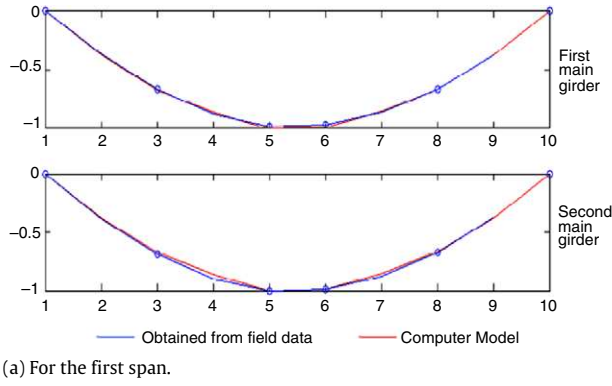


Fig. 20. Mode shapes obtained for the spans using the recorded acceleration data.

Table 4
Impact factors obtained from bridge tests.

Member type	Predicted under current train traffic		
	Mean value	Maximum value	Standard deviation
Main girders	1.18	1.23	0.039
Floor beams	1.16	1.28	0.101
Stringers	1.15	1.30	0.117

Table 5
Minimum safety indices for the bridge.

Structural member	Minimum safety index
Main girders	7.69
Floor beams	6.07
Stringers	5.22

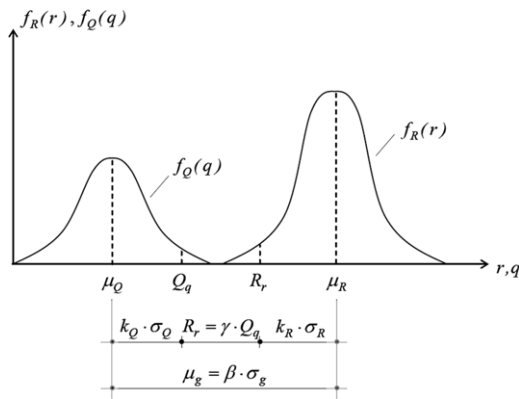


Fig. 21. Distribution of normal random variables R and Q .

A quantity g defined by Eq. (4) provides a quantitative measure of the probability of failure. The limit state is reached when $g = 0$. If $g > 0$, the structure is safe; whereas $g < 0$ means that the structure is unsafe. The quantity β is the quantitative measure of the probability of R exceeding Q and is usually referred to as the safety index. For normally distributed random variables R and Q , the safety index β can be represented by the following formula,

$$\beta = \frac{\mu_R - \mu_Q}{\sqrt{\sigma_R^2 + \sigma_Q^2}} \quad (5)$$

where μ_R and μ_Q are mean values, σ_R and σ_Q are standard deviations for the resistance and the load effect, respectively [17–20].

As shown in Fig. 21, the safety index, β based on safety factor, γ is presented by Roik [17] in the following expression,

$$\beta = \frac{\gamma(1 + k_Q V_Q) - (1 - k_R V_R)}{(1 + k_Q V_Q)\alpha_R V_R \gamma + (1 - k_R V_R)\alpha_Q V_Q} \quad (6)$$

in which,

$$\alpha_R = \frac{\sigma_R}{\sqrt{\sigma_R^2 + \sigma_Q^2}} \quad \text{and} \quad \alpha_Q = \frac{\sigma_Q}{\sqrt{\sigma_R^2 + \sigma_Q^2}} \quad (7)$$

$$k_R = \frac{\mu_R - R_r}{\sigma_R} \quad \text{and} \quad k_Q = \frac{Q_q - \mu_Q}{\sigma_Q} \quad (8)$$

$$\gamma = \frac{F_y/\omega}{\phi F_p + F_g} \quad (9)$$

where σ_R and σ_Q are standard deviations, μ_R and μ_Q are mean values, V_R and V_Q are coefficients of variations, R_r and Q_q are nominal values for the resistance and the load effect, respectively.

In order to calculate corresponding safety indices using the above referenced expression, the following statistical parameter values were selected,

$$k_Q = 1.2820 \quad \alpha_Q = 0.7100 \quad V_Q = 0.1256$$

$$k_R = 1.2820 \quad \alpha_R = 0.7100 \quad V_R = 0.1584.$$

Minimum values of calculated safety indices for the bridge members are presented in Table 5.

With a minimum safety index greater than $\beta = 3$ that has been determined by Turkish State Railways Administration for a UIC [13] train set by conducting dynamic tests on bridges to refine the initial computer models, the bridge was found to have no problem related to load carrying capacity. As a result of these proposed dynamic loads, fatigue-related issues were also investigated by the authors and remedies for deficient details were proposed in a previous study by Caglayan et al. [21]. To predict the spent fatigue life of the bridge, a numerical procedure based on Miner's linear damage accumulation theory [22] was used. Service life of the bridge was determined according to variable axle loads and conditions since construction date. Produced fatigue load profiles were loaded on the refined computer models and stress variations for each bridge member were computed. The most critical point was found to be the stringer-to-floor beam connection. For this critical joint, a stress histogram was prepared using the rainflow cycle counting method based on the stress values. Based on these calculations, accumulated fatigue damage for each bridge member was calculated. The same algorithm was applied for future UIC-based train traffic that has heavier axle loads to act more frequently than the current number of passages, and it was found that stringers would fail due to accumulated fatigue damage in less than 3 years. In the light of this output, a rehabilitation scheme was proposed [21].

8. Evaluation of the bridge for earthquake loading

Seismic evaluation of the bridge was performed according to the current national standards, namely the Specification for

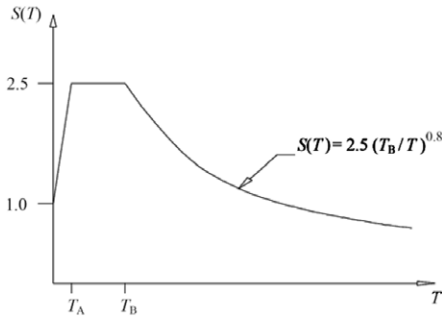


Fig. 22. The design acceleration spectrum.

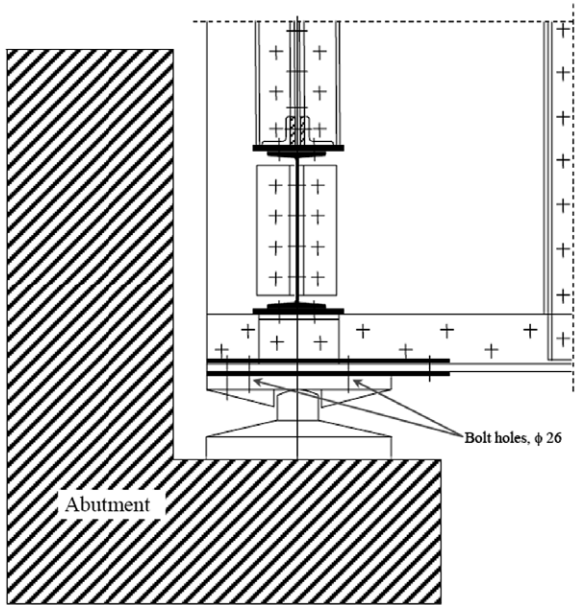


Fig. 23. Constructional detail of a pinned support.

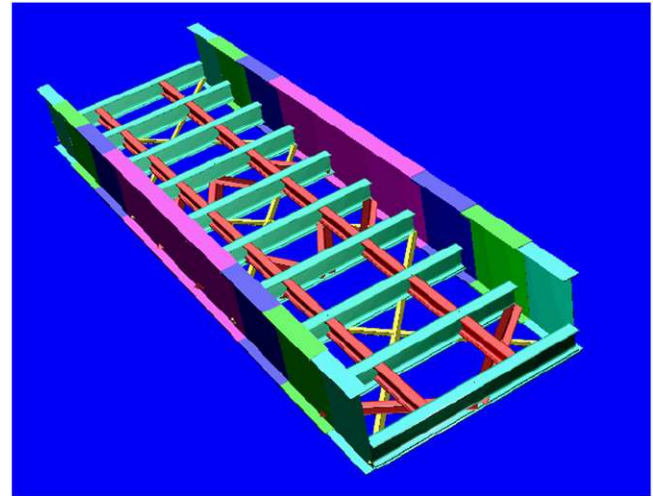


Fig. 25. Rendered finite element model of the reinforced bridge structure.

$$S(T) = 2.5 \left(\frac{T_B}{T} \right)^{0.8} \quad \text{if } T_B \leq T \quad (12)$$

where T_A and T_B are the spectrum characteristic periods depending on local site classes. For the soil class, Z3 that characterises highly weathered rock of the bridge location, T_A and T_B values are 0.15 s and 0.60 s, respectively.

By using the mode-superposition method within COSMOS/M [12] computer software, the bridge structure was analysed for the horizontal component of the design earthquake given by the aforementioned national standards.

Behaviour of supports realised from inspection of current situations and constructional drawings of mechanical supports are presented in Figs. 23 and 24, where two supports are pinned, with the remaining two supports free to translate and rotate in longitudinal direction of the bridge, whereas each one is restrained to translate in the transverse direction. However, one of the pinned support points has lost its character as a result of the catastrophic Kocaeli (Marmara) Earthquake of 1999, as shown in Fig. 24(b). Analyses results have shown that supports of the bridge were not satisfactory to transmit the earthquake-induced forces to the substructure in the longitudinal and transverse directions.

Instead of reinforcing these existing bridge supports under earthquake forces, additional supports, and seismic cross braces (see Figs. 25–28) were designed according to allowable stress criteria and for earthquake forces only in the longitudinal and transversal directions. The three-dimensional computer model of the reinforced bridge structure is given in Fig. 25. The additional and existing members of the reinforced bridge for earthquake forces are presented in Fig. 26, where member 3 denotes existing horizontal cross bracing. Member 1 shows the additional braces with a 2L100.100.10 cross-section and numbers 4 and 5 show additional support locations. To withstand train brake loads, members denoted by 2 are used.

9. Lateral buckling load capacity of the compression flange of the main girders located on the fourth span

Due to the truck collision, permanent deformations at each main girder of the fourth span have occurred with the shape of a half sine wave in the horizontal plane (see Fig. 29). Due to this excessive initial imperfection, reduction in lateral buckling capacity of the girder is obvious. In order to calculate the extent of reduction, lateral rigidity of the frame portion around the floor beam to main girder connection was calculated.

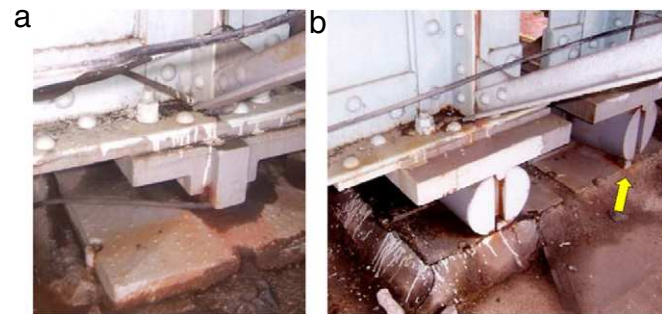


Fig. 24. Views of normal and problematic supports of the bridge.

Structures to be Built in Disaster Areas [23]. According to this specification, the effective ground acceleration coefficient, A_0 was taken as 0.4g, where g is the acceleration due to gravity. Seismic importance factor, I , was assumed as 1.5. Structural behaviour factor, R , of the bridge was taken as 1.0. The design acceleration spectrum, $S(T)$ is given in Fig. 22.

The design acceleration spectrum, $S(T)$, which depends on the bridge site conditions and the natural periods of the bridge, T , is determined by using the following formulae;

$$S(T) = 1 + 1.5 \frac{T}{T_A} \quad \text{if } 0 \leq T \leq T_A \quad (10)$$

$$S(T) = 2.5 \quad \text{if } T_A \leq T \leq T_B \quad (11)$$

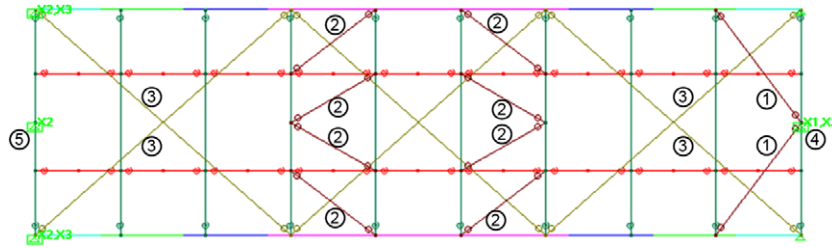


Fig. 26. Plan view of reinforced bridge structure.

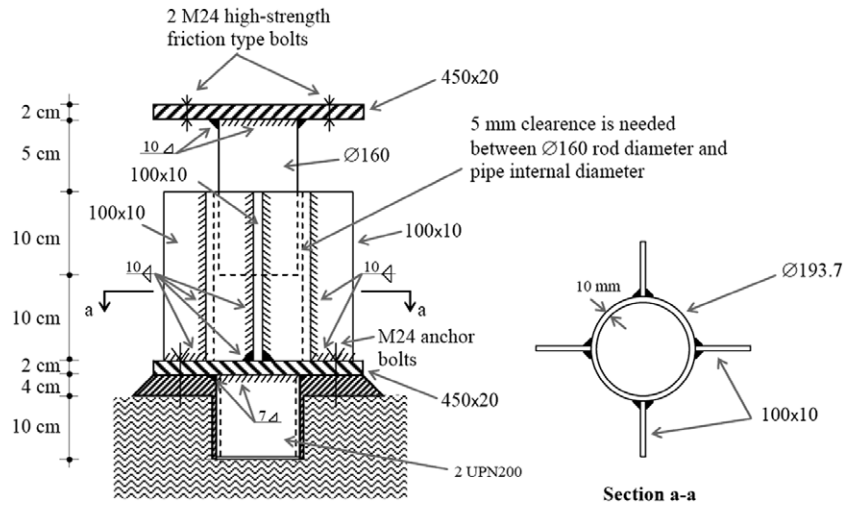


Fig. 27. Constructional drawing of the additional support 4.

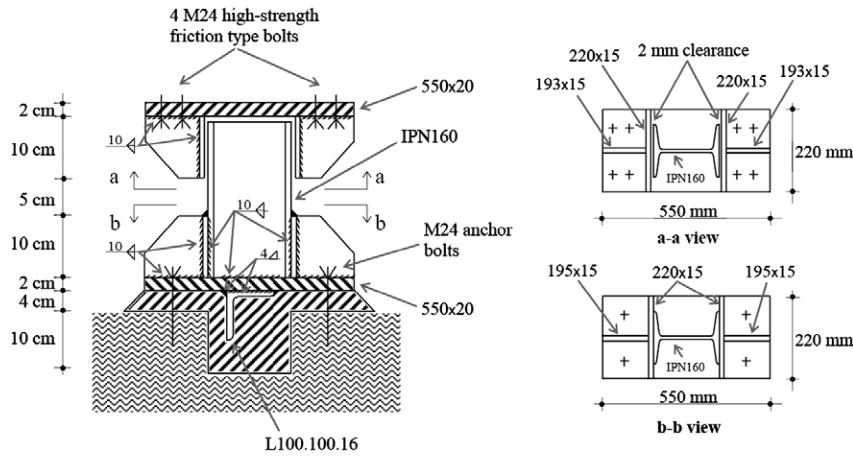


Fig. 28. Constructional drawing of the additional support 5.



Fig. 29. Deformed main girder of the fourth span.

The connection detail was idealised as shown in Fig. 30(b). Beam elements were used that passed along the main axes of the floor beam and the main girder, with a rotational spring for interconnection. A notional horizontal load of 10 kN was applied and displacement in the direction of this load was found as 0.0213 cm. Dividing these values has resulted in an equivalent lateral stiffness of 469 kN/cm. Using this value, two models representing as-built and crooked conditions of the fourth span were prepared. Schematic description of these models are outlined below in Fig. 31. Flange and one-third of the compressive area of the web (one-sixth of web depth) were assumed to resist lateral buckling, as specified by Eurocode 3 [24] and is shown in Fig. 32.

Employing the geometrically nonlinear buckling analysis algorithm of the COSMOS/M [12] finite element analysis software, critical buckling load, P_{cr} was found as 6390 kN for the first model

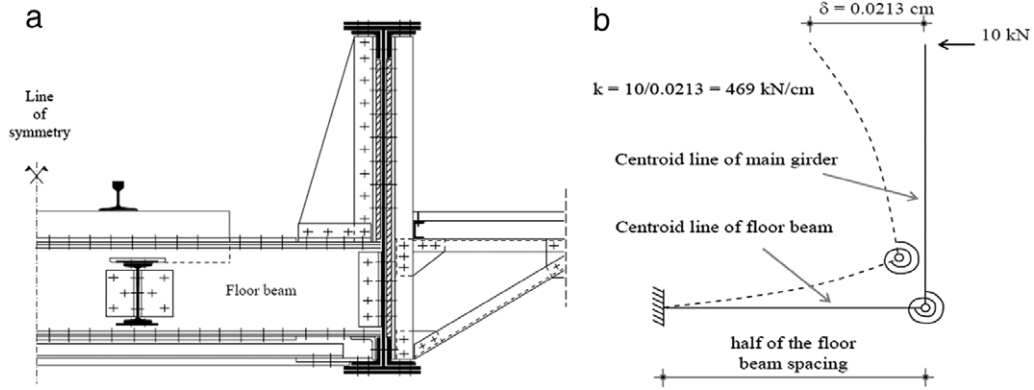
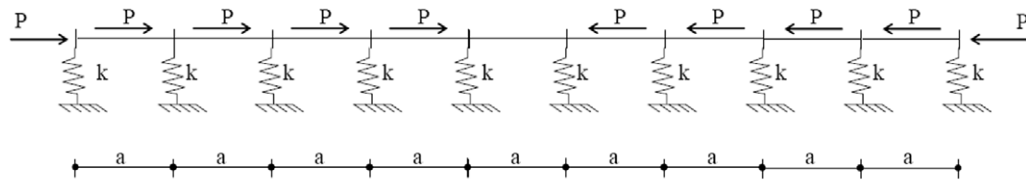


Fig. 30. Detail of floor beam to main girder connection.



a = 150 cm (floor beam spacing)
 (a) Model 1 has no significant initial imperfection.

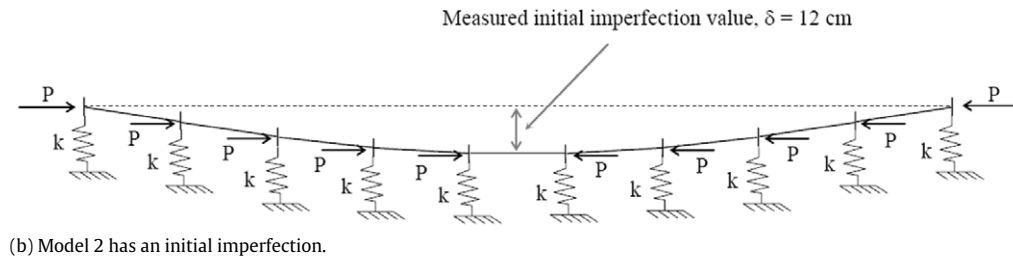


Fig. 31. Compressive flange of the main girder as lateral buckling member models.

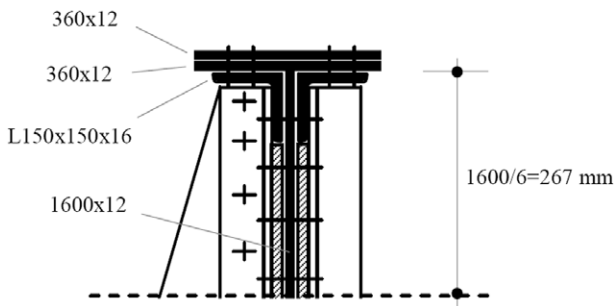


Fig. 32. Compressive flange cross-section taken into account for the main girder.

(no imperfection) and 503 kN for the second model (permanent deformation case).

Results indicate that, existence of this permanent deformation has caused 92% reduction in lateral buckling load capacity of compression flange of main girders. Therefore, it was concluded that the only choice was to write off the bridge segment on fourth span.

10. Conclusion

In this study, assessment of a railway steel bridge was conducted for train-induced loads and seismic actions. A 3D computer

model of the bridge was generated and validated based on dynamic field measurements and laboratory tests. The calibrated model of the bridge structure was then used for necessary calculations regarding structural assessment and evaluations according to train and seismic loads.

For earthquake loading with respect to current national specification, it was concluded that existing supports were not able to transmit the earthquake forces to abutments and pier safely. In order to provide safe transmission of these support forces, additional supports and horizontal cross members were suggested. Also, the damaged cross bracing members were replaced accordingly.

For the existing permanent deformation in upper and lower flanges, buckling analyses were performed. It was found that the imperfection of the flanges of the main girders of the fourth span causes 92% reduction in buckling load capacity. Replacing the bridge on fourth span was deemed necessary based on this value.

References

- [1] Ermopoulos J, Spyrakos CC. Validated analysis and strengthening of a 19th century railway bridge. *Engineering Structures* 2006;28:783–92.
- [2] Spyrakos CC, Raftoyiannis IG, Ermopoulos JC. Condition assessment and retrofit of a historic steel-truss railway bridge. *Journal of Constructional Steel Research* 2004;60:1213–25.
- [3] Schlune H, Plos M, Gylltoft K. Improved bridge evaluation through finite element model updating using static and dynamic measurements. *Engineering Structures* 2009;31:1477–85.

- [4] Rebelo C, Simoes da Silva L, Rigueiro C, Pircher M. Dynamic behaviour of twin single-span ballasted railway viaducts-field measurements and modal identification. *Engineering Structures* 2008;30:2460–9.
- [5] Calcada R, Cunha A, Delgado R. Dynamic analysis of metallic arch railway bridge. *Journal of Bridge Engineering*, ASCE 2002;7(4):214–22.
- [6] Maragakis EM, Douglas BM, Chen Q. Full-scale field failure tests of railway bridge. *Journal of Bridge Engineering*, ASCE 2001;6(5):356–62.
- [7] Chajes MJ, Mertz DR, Commander B. Experimental load rating of a posted bridge. *Journal of Bridge Engineering*, ASCE 1997;2(1):1–10.
- [8] Wang X, Kangas S, Padur D, Liu L, Swanson JA, Helmicki AJ, Hunt VJ. Overview of a modal-based condition assessment procedure. *Journal of Bridge Engineering*, ASCE 2005;10(4):460–7.
- [9] Akgül F, Frangopol DM. Rating and reliability of existing bridges in a network. *Journal of Bridge Engineering*, ASCE 2003;8(6):383–93.
- [10] Itani AM, Bruneau M, Carden L, Buckle IG. Seismic behaviour of steel girder bridge superstructures. *Journal of Bridge Engineering*, ASCE 2004;9(3):243–9.
- [11] ASTM E8M-04. Test methods for tension testing of metallic materials (metric). Annual Book of ASTM Standards; 1997.
- [12] COSMOS/M. User's manual. Massachusetts (USA): Solidworks Corporation, Dassault Systèmes; 2008.
- [13] UIC. UIC 776-1 loads to be considered in railway bridge design. Paris (France): International Union of Railways Code; 1994.
- [14] BE. Railway bridge design. Berlin (Germany): German Standard Specification; 1960.
- [15] DIN 4114. Stability of steel members. Berlin (Germany): German Standard Specification; 1969.
- [16] Kim S, Nowak AS. Load distribution and impact factors for I-girder bridges. *Journal of Bridge Engineering*, ASCE 1997;2(3):97–104.
- [17] Roik K. Vorlesungen über stahlbau, grundlagen. Berlin (Germany): Verlag Von Wilhelm Ernst & Sohn; 1978.
- [18] Bakht B, Jaeger LG. Utilization of service loads in bridge evaluation. Dordrecht (Netherlands): Kluwer Academic Publishers; 1990.
- [19] Nowak AS, Collins KR. Reliability of structures. New York (USA): McGraw-Hill Companies, Inc.; 2000.
- [20] Frangopol DM, Strauss A, Kim S. Bridge reliability assessment based on monitoring. *Journal of Bridge Engineering*, ASCE 2008;13(3):258–70.
- [21] Caglayan BO, Ozakgul K, Tezer O. Fatigue life evaluation of a through-girder steel railway bridge. *Engineering Failure Analysis* 2009;16(3):765–74.
- [22] Miner MA. Cumulative damage in fatigue. *Journal of Applied Mechanics* 1945; 12:159–64.
- [23] Ministry of Public Works and Settlement. Specification for structures to be built in disaster areas. Ankara (Turkey): Government of Republic of Turkey; 1998.
- [24] Eurocode 3. Design of steel structures-part 1-1: general rules and rules of buildings. EN 1993-1-1. Brussels (Belgium): CEN, European Committee for Standardisation; 2005.